Persistence of the Topological Surface States in Bi$_2$Se$_3$ against Ag Intercalation at Room Temperature

Mao Ye,* Kenta Kuroda, Mikhail M. Otrokov, Anastasia G. Ryabishchenkova, Qi Jiang, Arthur Ernst, Evgueni V. Chulkov, Masashi Nakatake, Masashi Arita, Taichi Okuda, Tomohiro Matsushita, László Tóth, Hiroshi Daimon, Kenya Shimada, Yoshifumi Ueda, and Akio Kimura*

ACCESS | Metrics & More | Article Recommendations

ABSTRACT: The electronic and atomic structures of topological insulator Bi$_2$Se$_3$, upon Ag atom deposition, have been investigated by combined experimental methods of scanning tunneling microscopy (STM), photoelectron spectroscopy, and first-principles calculations. We show from the results of STM that the deposited Ag atoms are stabilized beneath the surface instead of being adsorbed on the topmost surface. We further reveal from the angle-resolved photoemission spectroscopy that the Bi$_2$Se$_3$(0001) topological surface states stay uninterrupted after a large amount of absorption of Ag atoms. Our analysis of the photoelectron intensity of Ag core states excited by soft X-ray suggests that a large amount of deposited Ag atoms diffused into a deeper place, which is beyond the probing depth of X-ray photoelectron spectroscopy. The first-principles calculations identify the octahedral site in the van der Waals gaps between quintuple layers to be the most favorable locations of Ag atoms beneath the surface, which yields good agreement between the simulated and experimental STM images. These findings pave an efficient way to tailor the local lattice structures of topological insulators without disturbing the topologically nontrivial surface states.
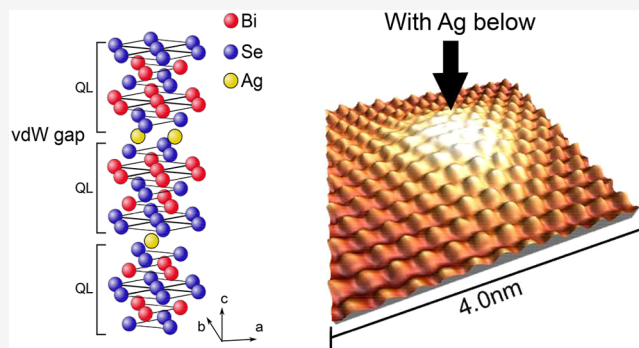
I. INTRODUCTION

A novel class of quantum materials, called topological insulators (TIs),[1,2] has provoked much research interest. A number of materials that hold nontrivial spin-polarized metallic surface states have been intensively studied, such as Bi$_{1-x}$Sb$_x$,[3−5] Bi$_2$Te$_3$,[6,7] Bi$_2$Se$_3$,[8−10] and thallium-based TIs,[11−16] among which Bi$_2$Se$_3$ is one of the most studied prototype materials due to a sufficiently large bulk energy gap.[8] because of time-reversal symmetry, topological electronic states are well protected from backscattering in the presence of impurities or defects. Such a unique property makes TIs robust against a materials' details, such as defects or impurities. However, a deeper insight into the interplay between the impurities and the local structures, such as the adsorption site and lattice modification, is still missing.

The intercalation of guest atoms has been widely applied to two-dimensional materials, which can effectively tailor the electronic structures, such as the modification of charge density wave in transition metal dichalcogenides via electron−phonon coupling,[17,18] as well as inducing strains to manipulate the band topologies.[19−21] For the TI materials, the copper-intercalated Bi$_2$Se$_3$ that induced superconducting transition coexisting with topological surface states has been extensively studied.[22−24] Besides, the intercalation of magnetic atoms has also been applied to enhance the optical performance of TIs.[25] On the other hand, implanting noble metals, such as silver, which has been widely used as a catalyst in different chemistry processes, may provide a novel opportunity to tailor the functionality of topological materials while maintaining their unique topological properties. In this study, we demonstrate that a numerous amount of silver atoms can be intercalated into the van der Waals (vdW) gaps of Bi$_2$Se$_3$ via evaporation of silver at room temperature as directly visualized by scanning tunneling microscopy. The angle-resolved photoelectron spectroscopy (ARPES) measurement reveals that the topological surface state of Bi$_2$Se$_3$ is not deteriorated by the intercalation of Ag atoms. The X-ray photoelectron spectroscopy (XPS) measurements further reveal that the intercalated Ag atoms can migrate to the deeper place of the crystal. Our
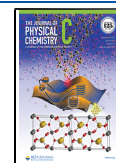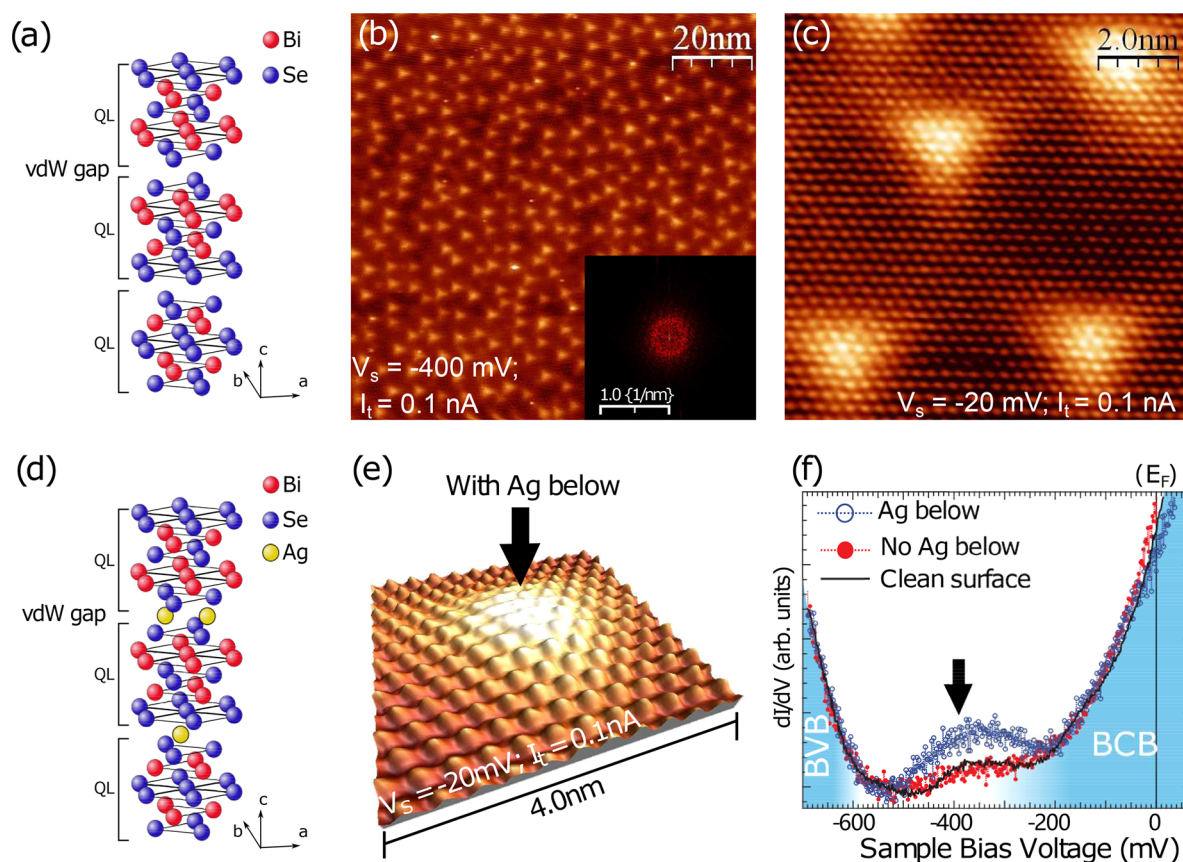
Figure 1. (a) Crystal structure of $Bi_2Se_3(0001)$. (b) Topography STM image of Ag-deposited Bi_2Se_3 surface with triangular-shaped corrugations in 100 nm × 100 nm area. Inset: Fourier transformed image of panel b. (c) Atomically resolved STM image of Ag deposited surface. (d) Schematic model of Ag-intercalated Bi_2Se_3. (e) 3D illustration of the magnified image of one of the convexities with Ag-intercalated below (marked by an arrow). (f) Spatially resolved tunneling spectra taken at the areas with (blue spectrum) and without (red spectrum, manually shifted by −40 mV) Ag atoms intercalated underneath, compared with the spectrum of clean surface (black spectrum, manually shifted by −135 mV).

first-principles calculations show that the Ag atoms can be stabilized at the octahedral site of the vdW gaps due to a substantial energy gain. These novel findings provide a deep insight into the interplay between topological materials and defects in a microscopic view of atomic and electronic structures, and thus open a pathway to engineering and tailoring the layered topological materials with novel functionalities, which will facilitate the realization of fault-tolerant quantum devices.[26]

II. EXPERIMENTAL METHODS

The single crystalline Bi_2Se_3 used in this research was grown by a standard Bridgman method. Stoichiometric mixtures of Bi (99.999%: shots, Mitsuwa) and Se (99.999%: shots, Mitsuwa) were melted in evacuated quartz ampules at 800 degrees at a pressure lower than 5×10^{-7} Torr for a day. Then they were slowly cooled over 3 days to 550 degrees, and this temperature was kept fixed for 24 h for the soft annealing of the samples. The samples were then gradually cooled to room temperature. The crystal was cleaved along the basal plane (111), producing a mirror-like surface. The band structures of the pristine Bi_2Se_3 samples have been obtained using synchrotron radiation ARPES as described elsewhere.[9] The deposition of Ag atoms was conducted by setting a small amount of Ag wire (99.99%, Nilaco) in a conventional filament basket made by tungsten wire. During the Ag deposition, the Bi_2Se_3 samples were kept at room temperature. The STM and scanning tunneling

spectroscopy (STS) measurements were performed with a commercial low-temperature STM (LT-STM, Omicron). The sample was cooled to 78 K by liquid nitrogen during STM/STS measurement. The STM images presented in this work were all taken in a constant current mode with an electrochemically etched tungsten tip, and processed using the WSxM applications.[27] The STS data and differential conductance map were collected with a standard lock-in technique working at a frequency of 1.0 kHz and modulation amplitude of 10 mV. The ARPES data were collected at the undulator beamline BL-9A of Hiroshima Synchrotron Radiation Center (HSRC) with a hemispherical photoelectron analyzer (VG-SCIENTA R4000). During the experiments, the energy and angular resolutions were set to be 8−15 meV and 0.2 degree, respectively. The XPS measurements on the core level states were performed at the bending magnet beamline BL-7 of HSRC also with a hemispherical photoelectron analyzer (VG-SCIENTA 2002). The X-ray photoelectron diffraction (XPD) experiments were performed at the University of Tokyo Synchrotron Radiation Outstation Beamline BL07LSU at SPring-8 using the Display-type Ellipsoidal Mesh Analyzer (DELMA) spectrometer[28] at room temperature.
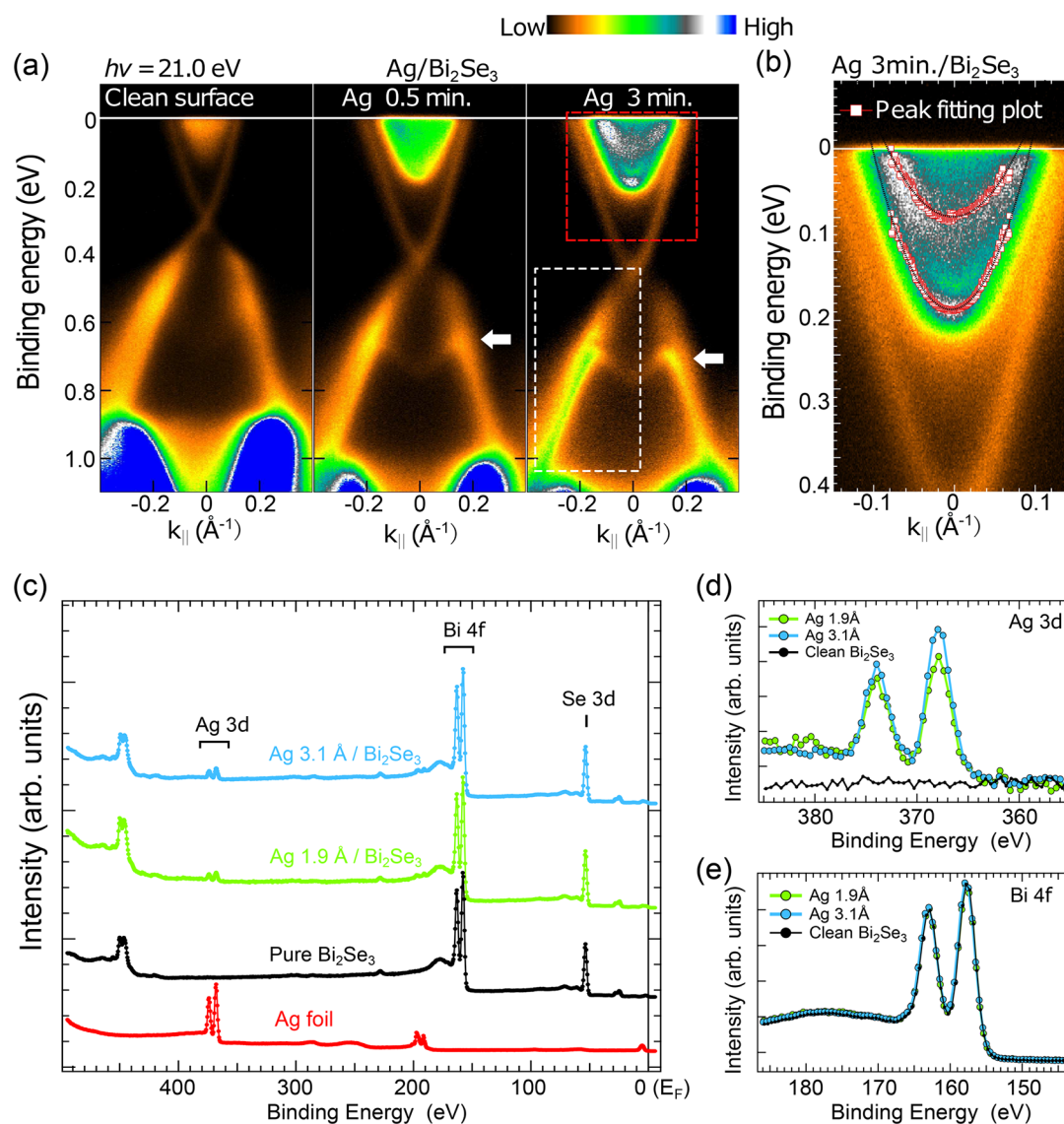
Figure 2. (a) Band structures of $Bi_2Se_3(0001)$ with the increase of the Ag deposition time from 0.5 to 3 min measured by ARPES with a photon energy of 21.0 eV. (b) Expanded image of the red dashed box in panel a with superimposed EDC peak dispersion plots (red squares). (c) XPS spectra of Ag-deposited Bi_2Se_3 surface with a Ag amount of 0, 1.9, and 3.1 Å measured with 550 eV photons compared with Ag polycrystal foil measured under the same condition. (d,e) Core level spectra of (d) Ag 3d and (e) Bi 4f states normalized by Se 3d intensity.

III. SURFACE TOPOGRAPHY OF SILVER-ADSORBED BI_2SE_3

The crystal structure of Bi_2Se_3 is built of quintuple layer (QL) units spaced by van der Waals (vdW) gaps, where each QL consists of hexagonal atomic layers in the order of Se−Bi−Se−Bi−Se, as depicted in Figure 1a. Hence, the clean surface obtained by *in situ* cleavage in ultrahigh vacuum exposes the topmost Se layer of the QL. For the as-cleaved Bi_2Se_3 surface, some clover-shaped defects due to the substitutional Bi atoms or a vacancy at the Se-site can be observed by STM, which introduce extra carriers that make the Bi_2Se_3 crystals intrinsically n-doped, as reported previously.[29,30] Figure 1b shows a typical topographic STM image of the Bi_2Se_3 surface measured at 78 K after the deposition of Ag at room temperature. The surface is seen to be dominated by triangular-shaped bright spots. The analysis of the topographic image by Fourier transformation (inset of Figure 1b) reveals a circular shaped intensity distribution in the center of the transformed image, the 0.176 nm^{-1} radius of which does not

depend on the sample bias voltage. This means that the randomly distributed triangular-shaped convexities on the surface maintain a typical distance approximately 5.7 nm from each other. The atomically resolved STM image of a smaller region is shown in Figure 1c. The 6-fold symmetry arrangement of Se lattice on the topmost surface is clearly seen. More importantly, the Se layer appears as a periodic lattice continuously spreading over the surface with triangular-shaped convexities, indicating that all the Ag atoms are beneath the topmost layer. It is reasonable to suppose that Ag atoms are intercalated in the vdW gaps between QLs of Bi_2Se_3 crystal (Figure 1d) due to the weak bonding. This point will be thoroughly discussed later. Figure 1e shows a three-dimensional (3D) image of a small-area scan containing one of the triangular-shaped regions in Figure 1c. The surface Se layer is seen to be slightly protruded due to the Ag atoms underneath. The bright region in this figure, indicated by a black arrow, corresponds to the area with buried Ag atoms.
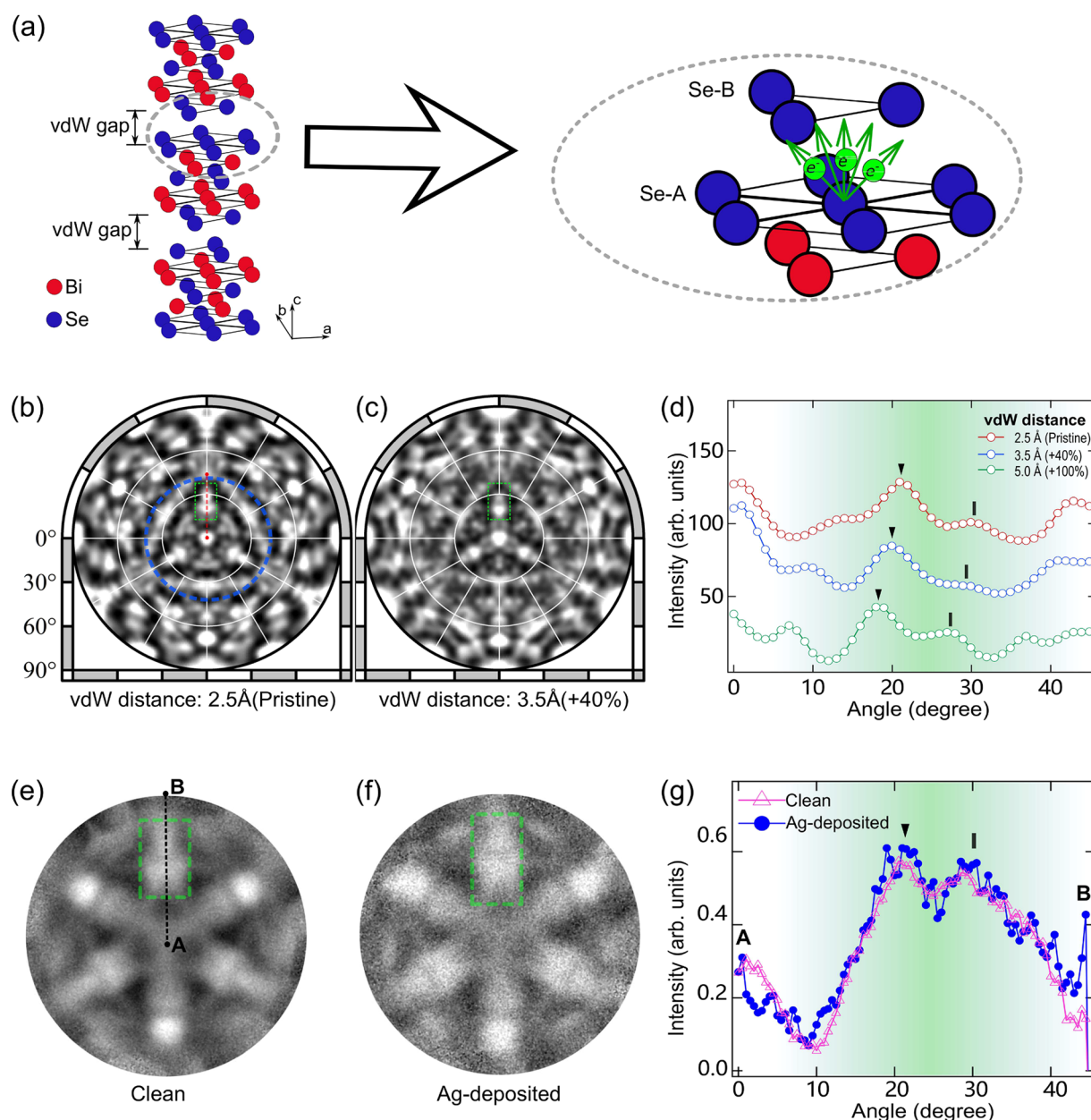
Figure 3. (a) Lattice structure of Bi_2Se_3, the atomic layers at the vicinity of vdW gap (indicated in the gray dashed ellipse) are magnified at the right, where the Se atoms acting as the photoelectron emitter are indicated as Se-A. (b,c) Simulated XPD patterns of Se 3d photoelectrons at E_K of 600 eV with vdW distance of 2.5 Å (pristine) and 3.5 Å (expanded by 40%). (d) Intensity line-profile of the simulated XPD pattern along the red dashed line in panel b for vdW distances of 2.5, 3.5, and 5.0 Å. The experimentally measured XPD patterns of Se 3d photoelectrons (e) before and (f) after Ag deposition. (g) Intensity line-profile obtained in panels e and f; see text.

To further explore the electronic states of the Ag-deposited Bi_2Se_3 surface, we have measured the spatially resolved differential conductance spectra of this surface. They are known to reflect to a good approximation the local density of states of the probed surface area.[31] The spectra shown in Figure 1f are taken in the region with (blue) and without (red) Ag underneath, corresponding to the bright and dark areas in the topographic image, respectively. Also the spectrum taken on the clean Bi_2Se_3 surface is shown for comparison. The steep edges below and above the energy gap in the three dI/dV spectra coincide to each other by applying the energy shifts of −40 meV and −135 meV to the spectrum taken at the area without Ag below (red spectrum) and the spectrum taken at the clean surface (black spectrum), respectively. The energy

shift of ~135 mV between the spectrum of the area with Ag and the clean surface is ascribed to the electron doping due to Ag intercalation, while the small shift of ~40 mV between the spectra of the areas with and without Ag atoms is caused by the spatially local energy shift of the electron states relative to the Fermi level (E_F) due to the influence of the intercalated Ag atoms.

Note that the structure of the dI/dV curve of the Ag-doped surface (Figure 1f) in the bulk energy gap is quite different from that of the clean surface. In the region with Ag (blue), the spectrum has a pronounced W-like shape with an intensity enhancement around −400 mV marked by a black arrow, in contrast to the V-shaped spectrum of the clean surface (black solid line).

IV. SURFACE ELECTRONIC STRUCTURES OF SILVER-ADSORBED BI$_2$SE$_3$

To see the influence of the doped Ag on the electronic states of Bi$_2$Se$_3$, we have performed an angle resolved photoelectron spectroscopy (ARPES) measurement. Figure 2a shows the ARPES images exhibiting the time evolution of the surface band structure upon Ag deposition taken with a photon energy of $h\nu$ = 21 eV. In the case of the clean surface, the cone-shaped dispersion is clearly seen with the Dirac point located at a binding energy (E_B) of 300 meV. Simultaneously, the bulk conduction band can be observed near the E_F with the band bottom located at E_B = 120 meV. After depositing a small amount of Ag on the surface (deposition time, ∼0.5 min) both the bulk and the surface bands shift by 60 meV. The energy shift stabilizes at 80 meV after 3 min of Ag deposition. Besides, there appear two surface-state bands, which overlap with the bulk conduction band near the conduction band minimum (CBM), as indicated by the red dashed box in the rightmost graph of Figure 2a. Meantime, there also appears a set of M-shaped band overlapping with the bulk valence band after Ag-deposition, as indicated in the white dashed box in Figure 2a. An expanded image near the CBM is shown in Figure 2b, where the peak positions fitted from energy distribution curves (EDC) are plotted by red square marks. The band bottoms of these two bands are determined as E_B = 79 and 186 meV by fitting the plots with two parabolic curves (black dashed lines). These newly developed electronic states in the valence and conduction bands can be ascribed to the slight expansion of van der Waal's gaps of Bi$_2$Se$_3$ after Ag adsorption, as demonstrated by Eremeev et al., by means of relativistic *ab initio* calculations.[32]

The spectral weight of the background does not appreciably increase even after 5 min of Ag deposition, indicating a well preserved crystal structures of Bi$_2$Se$_3$ surface after a large amount of Ag adsorption. To further confirm the existence of Ag atoms deposited at the Bi$_2$Se$_3$ surface, we investigated the intensity of the Ag 3d core levels by X-ray photoelectron spectroscopy (XPS). Figure 2c shows the wide range XPS spectra of Bi$_2$Se$_3$ with different Ag deposition amounts (0, 1.9, and 3.1 Å) measured with photon energy ($h\nu$) of 550 eV at room temperature. To confirm the core level states of Ag that emerged after Ag deposition at the Bi$_2$Se$_3$ surface, we have also measured polycrystal Ag foil as a reference as shown in red color in Figure 2c, where the Ag 3d states and the Auger electron peaks are present at an E_B of 380−360 and 195 eV, respectively. As one can see, the Ag 3d core level peaks, coexisting with the Bi 4f and Se 3d states, are clearly observed after Ag deposition, which evidenced the adsorption of Ag atoms at the Bi$_2$Se$_3$ surface. To analyze the evolution of Ag 3d states as a function of Ag coverage, the spectra are normalized by the intensity of the Se 3d peak located at an E_B of 56 eV. As shown in Figure 2d, when the deposition amount of Ag increased from 1.9 to 3.1 Å, the intensities of the Ag 3d peaks only show a small increase. This strongly indicates that the additionally deposited Ag from 1.9 to 3.1 Å diffused deeper than the mean-free-path of the photoelectrons, which is about ∼1 nm at this kinetic energy.[33] Moreover, the core level shapes of deposited Ag show negligible difference from those of the pure Ag foil, that is, neither shoulder structures nor energy shift emerges, indicating that the Ag atoms almost act as intact guest atoms after being deposited on Bi$_2$Se$_3$. This can also be verified by the core level spectra of Bi$_2$Se$_3$, such as Bi 4f (Figure 1c),

where no additional shoulder structure appears after the deposition of Ag.

To further reveal the influence of the Ag atom adsorption at the Bi$_2$Se$_3$ surface, we performed X-ray photoelectron diffraction measurements to probe the local structure variation before and after Ag adsorption. It was predicted by Otrokov et al. that the octahedral position inside the vdW gap may be the most stable site for Ag atoms due to the lowest total energy.[34] However, the existence of Ag atoms inside the vdW gaps might result in an expansion of the vdW gaps between the QLs of Bi$_2$Se$_3$, which is closely related to the energy band topology. We then measured the diffraction patterns of the photoelectrons emitted from the Se atoms just below and above the vdW gap (Se-A and Se-B in Figure 3a). In case there is an expansion of the vdW gap, the distance between Se-A and Se-B will be elongated, resulting in the changes of the intensity distribution for the forward-focusing-peak (FFP) in the XPD patterns.[28,35]

Figure 3 panels b and c compare the simulated XPD patterns of Bi$_2$Se$_3$ generated by the diffraction of the Se 3d core level photoelectrons without and with vdW gap expansion, where the FFP originated from the Se-B site is indicated in the green dashed boxes. To see the effect by the expansion of the vdW gap, we then compared the intensity line profiles along the red dashed line indicated in Figure 3b. As can be clearly observed in Figure 3d, the two peaks indicated by black triangles and sticks systematically shift toward small angle with increasing vdW distance. This is due to the increasing distance between the Se-A and Se-B atoms, which will subsequently result in a decrease of emission angle of the FFP generated by the Se 3d core level photoelectrons from the Se-A site in the XPD patterns. Figure 3 panels e and f show the experimentally probed XPD patterns in the region indicated by a blue dashed circle in Figure 3b using the Se 3d core level photoelectrons at kinetic energy (E_K) of 600 eV, which shows excellent agreement with the simulated patterns in the corresponding region in Figure 3b. The FFP spots generated by the Se−B site are also clearly probed in the XPD patterns both before and after the Ag deposition as indicated by the green dashed boxes in Figure 3e,f. To examine whether this FFP spot changes upon the Ag deposition, we quantitatively compared the intensity line profiles indicated by the black dashed line in Figure 3e before and after the Ag deposition. As shown in Figure 3g, the area indicated by the green shadow corresponds to the FFP intensity from the Se-B site as shown in the green dashed boxes in Figure 3e,f. However, these intensity profiles show negligible change before and after the Ag deposition. Such result may also be understood from the STM images, where the deposition of Ag only results local protrusions on the surface. Most of the area on the surface, where no Ag atoms are intercalated, are left intact; that is, the distance between Se-A and Se-B may be elongated only at the local area where Ag atoms are intercalated. Since XPD experiment probes the averaged structural information on the whole surface, the local changes that occurred around the intercalated Ag atoms are probably smeared out. The results of the XPD measurements suggest that the adsorption of Ag atoms only results in a modification of local atomic structures, thus the topologically nontrivial surface states stay intact. This can be regarded as a manifestation of the robust topological properties that is insensitive to the details of materials, such as impurities or defects.
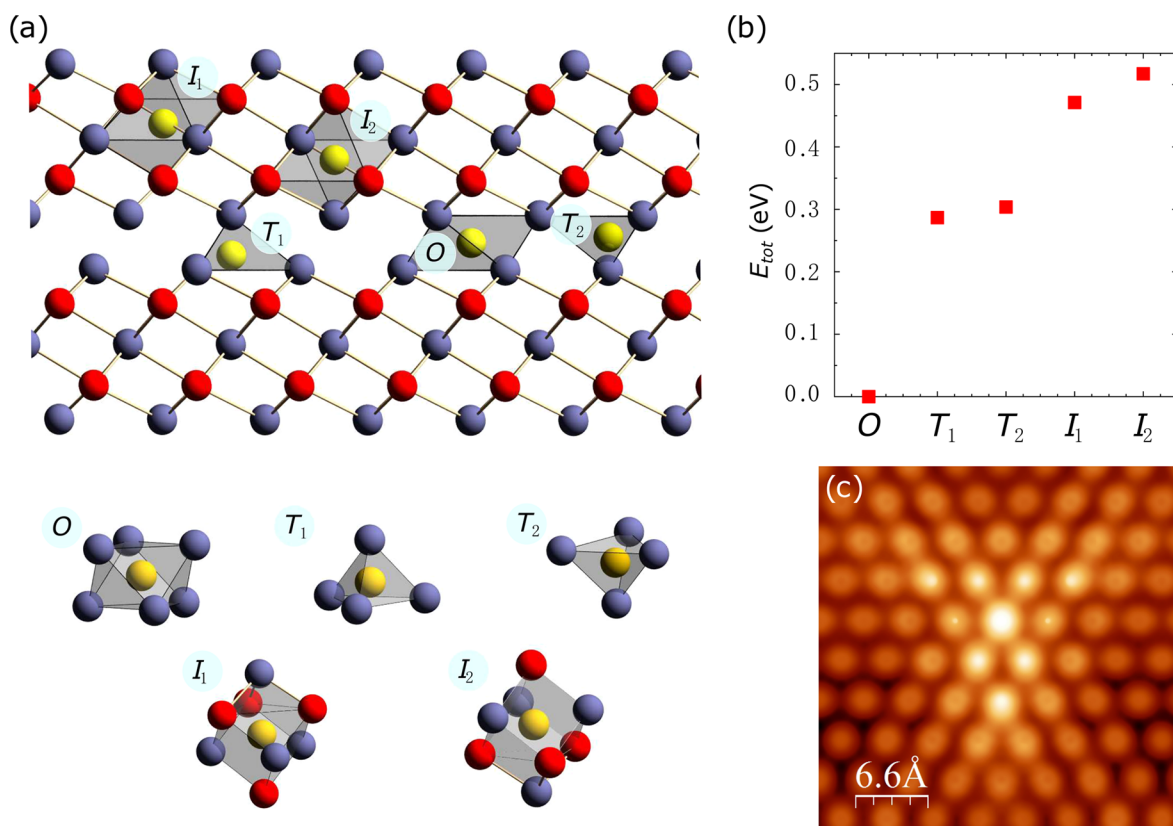
Figure 4. (a) Schematic side view of the two topmost QLs of the $Bi_2Se_3(0001)$ surface with possible interstitial locations of Ag atoms: octahedral (O) and tetrahedral (T_1 and T_2) vdW voids as well as the interstitial positions inside the topmost QL (I_1 and I_2). (b) Total energies calculated for the Ag atom located in the positions shown in panel a. The energy for the Ag atom in the octahedral vdW position O is taken as zero. (c) Simulated STM topographic image for the case of the Ag atom located in the O position.

V. THEORETICAL INVESTIGATION ON LOCAL ATOMIC AND ELECTRONIC STRUCTURES

The octahedral position inside the vdW gap (Figure 4a) was previously calculated to be the most energetically favorable site for an Ag atom among the surface/vdW sites at/below $Bi_2Se_3(0001)$.[34] Moreover, if the surface features a significant amount of the steps (which is typically the case for $Bi_2Se_3(0001)$[36,37]), such sites are expected to be readily accessible to the deposited Ag atoms via the step-mediated intercalation, as predicted in refs 34 and 38. These predictions are well in line with our experimental observations that indicate the subsurface location of Ag atoms. Besides, lately, an efficient Ag intercalation at room temperature into the vdW gaps of $Bi_{1.5}Sb_{0.5}Te_{1.7}Se_{1.3}$ has also been reported based on the results of the angle-resolved and core-level photoemission measurements.[39] However, a very recent surface X-ray diffraction study of the Ag-deposited $Bi_2Se_3(0001)$ reports rather different results.[40] For the Ar-ion-sputtered (0001) surface of a Bi_2Se_3 single crystal annealed at 480 °C, the Ag atoms deposited at room temperature are found to both substitute Bi atoms within the first QL and reside in the surface hollow sites. On the contrary, when Ag is deposited on an epitaxially grown $Bi_2Se_3(0001)$ film that has only been annealed at 400–450 °C prior to the deposition (i.e., there has been no sputtering treatment), only adsorption in the surface hollow sites is observed. The differences in the reactivity of the two surfaces have been attributed to the creation of defects by sputtering that might facilitate the occupation of Bi sites by Ag atoms.[40] However, no Ag

intercalation into the Bi_2Se_3 vdW gap has been found by the authors of ref 40 neither with sputtering of the surface nor without it. Concerning these results, we note that no sputtering or annealing has been used in our experiments whereby the occupation of the Bi sites by Ag seems unlikely. Nevertheless, to shed more light on the localization of the Ag atoms, we have performed first-principles calculations using the projector augmented-wave method[41,42] as implemented in the VASP code.[43,44] The exchange-correlation energy has been treated using the generalized gradient approximation.[45] To describe the vdW interactions we have made use of the DFT-D3 approach,[46,47] which has been successfully applied to various vdW systems.[48–50] We find that this approach works good as far as the description of the Bi_2Se_3 bulk crystal structure is concerned, a full optimization yielding the structure parameters in good agreement with recent X-ray diffraction data.[51] To determine the equilibrium positions of the Ag atoms near the $Bi_2Se_3(0001)$ surface, we have chosen a (3×3) hexagonal plane cell, while for the STM simulations a $(8 \times 5\sqrt{3})$ rectangular cell has been chosen. In both cases, the cells contained two QLs and a vacuum layer with a thickness of no less than 10 Å. The selenium layer of the lower surface of the Bi_2Se_3 film has been fixed upon relaxation. In the (3×3) cell, the optimization of atomic positions continued until forces acting on each atom (except for the fixed Se atoms) become smaller than 0.025 eV/Å, while the atomic coordinates in the larger $(8 \times 5\sqrt{3})$ cell have been optimized with a tolerance criterion of 0.05 eV/Å and only a few atomic shells have been

allowed to move. No native defects of Bi_2Se_3 such as vacancies or antisite atoms have been considered in the calculations.

We first theoretically consider a scenario mimicking that of ref 40, in which Ag atoms occupy Bi sites in the subsurface atomic layer. We find that in such a case the Ag atoms provide holes in the system, which is in a stark contrast to the electron doping that we observe after the Ag deposition (see Figure 2a). Besides, our nudged elastic band calculations[52,53] of the reaction in which an Ag atom, deposited on $Bi_2Se_3(0001)$, and a Bi atom from the subsurface layer exchange their sites yield a large value of the activation energy (~2.2 eV) for such a process. Therefore, we can safely discard the scenario of a massive occupation of Bi sites by Ag atoms in our experiment. Then, since our STM measurements do not reveal Ag atoms at the surface, we further concentrate on the theoretical consideration of other potential locations of Ag below the surface. Our total energy calculations reveal that among all of the interstitial positions shown in Figure 4a the octahedral vdW site turns out to be by at least 0.286 eV more favorable than any other site (Figure 4b). At that, the interstitial positions inside the QL appear to be the most unfavorable. The STM topograph image, theoretically simulated in the Tersoff-Hamann approximation for the Ag atom located in the octahedral vdW site is shown in Figure 4c. One can see a bright triangular-shaped feature centered at the location of the Ag atom. Both the appearance and extension (~2.5−3 nm) of the feature fit well those of the experimentally observed triangular-shaped convexities. Note that our STM simulations reveal that at least for one of the tetrahedral sites (T_1) there is a triangular-shaped feature as well, the extension of which is similar to that found for the octahedral site (due to the same subsurface depth). We therefore only limit to stating that, in the case of the octahedral vdW site, *which is the most energetically favorable site*, the theoretically simulated STM topograph is compatible to the experimentally measured one. Thus, based on all the experimental and theoretical data presented, we conclude that Ag atoms indeed appear to be intercalated in the vdW gap of Bi_2Se_3. It should be noted that the limited size of the triangular-shaped convexities also indicates that the intercalation of the Ag atom only affects the local atomic structures, which is in agreement with our XPD measurements. We estimate the upper limit of the vdW gap expansion at the Ag location as 11%, as calculated in the (3×3) supercell, in which, unlike the ($8 \times 5\sqrt{3}$) cell, all atoms were allowed to move (except for the lowest Se layer of the film). Concerning a possible vdW expansion out of the triangular-shaped convexity region, we observe that in the calculation performed using the ($8 \times 5\sqrt{3}$) cell the forces acting on the majority of the vdW Se atoms are smaller than 0.05 eV/Å. The latter means that if those Se atoms were allowed to relax, they would likely experience only moderate or small shifts. Thus, the vdW gap of the Ag-intercalated Bi_2Se_3 should largely stay unexpanded so that the topology of the material, that is sensitive to the vdW gap size, should not be affected, as we indeed see in our ARPES experiments, evidencing the presence of the topological surface state. This is a manifestation of the robust properties of a topologically nontrivial state that is insensitive to materials' details, which suggests the possibility of implanting not only silver but also other functional atoms or clusters into topological materials by van der Waals gap intercalation, while maintaining the unique topological properties.

VI. CONCLUSION

We have experimentally demonstrated the persistence of the topological surface states on the (0001) surface of Bi_2Se_3 against the Ag deposition at room temperature. Our scanning tunneling microscopy and photoelectron spectroscopy measurements suggest an intercalation of Ag atoms below the $Bi_2Se_3(0001)$ surface. The first-principles calculations identify the octahedral site in the van der Waals gaps between quintuple layers to be the most favorable locations of Ag atoms beneath the surface, which is further evidenced by the good agreement between the simulated and experimental STM images. These findings demonstrate an efficient way to tailor the local lattice structures of TIs without disturbing the topologically nontrivial surface states.

■ AUTHOR INFORMATION

Corresponding Authors

Mao Ye − *State Key Laboratory of Functional Materials for Informatics, Shanghai Institute of Microsystem and Information Technology, Chinese Academy of Sciences, Shanghai 200050, China; Graduate School of Science, Hiroshima University, Higashi-Hiroshima 739-8526, Japan;* orcid.org/0000-0002-3298-4724; Email: yemao@mail.sim.ac.cn

Akio Kimura − *Graduate School of Science, Hiroshima University, Higashi-Hiroshima 739-8526, Japan;* orcid.org/0000-0002-1501-3918; Email: akiok@hiroshima-u.ac.jp

Authors

Kenta Kuroda − *Graduate School of Science, Hiroshima University, Higashi-Hiroshima 739-8526, Japan*

Mikhail M. Otrokov − *Centro de Física de Materiales (CFM-MPC), Centro Mixto CSIC-UPV/EHU, Donostia-San Sebastián, Basque Country 20018, Spain; IKERBASQUE, Basque Foundation for Science, Bilbao, Basque Country 48011, Spain; Donostia International Physics Center (DIPC), Donostia-San Sebastián, Basque Country 20018, Spain*

Anastasia G. Ryabishchenkova − *A.V. Rzhanov Institute of Semiconductor Physics, Siberian Branch of Russian Academy of Sciences, Novosibirsk 630090, Russia; Tomsk State University, Tomsk 634050, Russia*

Qi Jiang − *State Key Laboratory of Functional Materials for Informatics, Shanghai Institute of Microsystem and Information Technology, Chinese Academy of Sciences, Shanghai 200050, China*

Arthur Ernst − *Institut für Theoretische Physik, Johannes Kepler Universität, Linz A 4040, Austria; Max-Planck-Institut für Mikrostrukturphysik, Halle D-06120, Germany*

Evgueni V. Chulkov − *Departamento de Física de Materiales, UPV/EHU, Donostia-San Sebastián, Basque Country 20080, Spain; Donostia International Physics Center (DIPC), Donostia-San Sebastián, Basque Country 20018, Spain; Saint Petersburg State University, Saint Petersburg 198504, Russia*

Masashi Nakatake − *Hiroshima Synchrotron Radiation Center, Hiroshima University, Higashi-Hiroshima 739-0046, Japan*

Masashi Arita − *Hiroshima Synchrotron Radiation Center, Hiroshima University, Higashi-Hiroshima 739-0046, Japan*

Taichi Okuda − *Hiroshima Synchrotron Radiation Center, Hiroshima University, Higashi-Hiroshima 739-0046, Japan*

Tomohiro Matsushita − *Nara Institute of Science and Technology (NAIST), Ikoma, Nara 630-0192, Japan*

László Tóth − *Nara Institute of Science and Technology (NAIST), Ikoma, Nara 630-0192, Japan*

Hiroshi Daimon − *Nara Institute of Science and Technology (NAIST), Ikoma, Nara 630-0192, Japan*

Kenya Shimada − *Hiroshima Synchrotron Radiation Center, Hiroshima University, Higashi-Hiroshima 739-0046, Japan;* orcid.org/0000-0002-1945-2352

Yoshifumi Ueda − *Kure National College of Technology, Kure 737-8506, Japan*

Complete contact information is available at:
https://pubs.acs.org/10.1021/acs.jpcc.0c07462

Notes
The authors declare no competing financial interest.

REFERENCES

(1) Zhang, H.; Liu, C.-X.; Qi, X.-L.; Dai, X.; Fang, Z.; Zhang, S.-C. Topological insulators in Bi_2Se_3, Bi_2Te_3 and Sb_2Te_3 with a single Dirac cone on the surface. *Nat. Phys.* **2009**, *5*, 438.

(2) Hasan, M. Z.; Kane, C. L. *Colloquium*: Topological insulators. *Rev. Mod. Phys.* **2010**, *82*, 3045−3067.

(3) Hsieh, D.; Xia, Y.; Wray, L.; Qian, D.; Pal, A.; Dil, J. H.; Osterwalder, J.; Meier, F.; Bihlmayer, G.; Kane, C. L.; et al. Observation of unconventional quantum spin textures in topological insulators. *Science* **2009**, *323*, 919−922.

(4) Roushan, P.; Seo, J.; Parker, C. V.; Hor, Y. S.; Hsieh, D.; Qian, D.; Richardella, A.; Hasan, M. Z.; Cava, R. J.; Yazdani, A. Topological surface states protected from backscattering by chiral spin texture. *Nature* **2009**, *460*, 1106−1109.

(5) Nishide, A.; Taskin, A. A.; Takeichi, Y.; Okuda, T.; Kakizaki, A.; Hirahara, T.; Nakatsuji, K.; Komori, F.; Ando, Y.; Matsuda, I. Direct mapping of the spin-filtered surface bands of a three-dimensional quantum spin Hall insulator. *Phys. Rev. B: Condens. Matter Mater. Phys.* **2010**, *81*, No. 041309(R).

(6) Chen, Y. L.; Analytis, J. G.; Chu, J.-H.; Liu, Z. K.; Mo, S.-K.; Qi, X. L.; Zhang, H. J.; Lu, D. H.; Dai, X.; Fang, Z.; et al. Experimental Realization of a Three-Dimensional Topological Insulator, Bi_2Te_3. *Science* **2009**, *325*, 178−181.

(7) Zhang, T.; Cheng, P.; Chen, X.; Jia, J.-F.; Ma, X.; He, K.; Wang, L.; Zhang, H.; Dai, X.; Fang, Z.; et al. Experimental demonstration of topological surface states protected by time-reversal symmetry. *Phys. Rev. Lett.* **2009**, *103*, 266803.

(8) Xia, Y.; Qian, D.; Hsieh, D.; Wray, L.; Pal, A.; Lin, H.; Bansil, A.; Grauer, D.; Hor, Y. S.; Cava, R. J.; et al. Observation of a large-gap topological-insulator class with a single Dirac cone on the surface. *Nat. Phys.* **2009**, *5*, 398−402.

(9) Kuroda, K.; Arita, M.; Miyamoto, K.; Ye, M.; Jiang, J.; Kimura, A.; Krasovskii, E. E.; Chulkov, E. V.; Iwasawa, H.; Okuda, T.; et al. Hexagonally Deformed Fermi Surface of the 3D Topological Insulator Bi_2Se_3. *Phys. Rev. Lett.* **2010**, *105*, No. 076802.

(10) Zhang, Y.; He, K.; Chang, C.-Z.; Song, C.-L.; Wang, L.-L.; Chen, X.; Jia, J.-F.; Fang, Z.; Dai, X.; Shan, W.-Y.; et al. Crossover of the three-dimensional topological insulator Bi_2Se_3 to the two-dimensional limit. *Nat. Phys.* **2010**, *6*, 584−588.

(11) Yan, B.; Liu, C.-X.; Zhang, H.-J.; Yam, C.-Y.; Qi, X.-L.; Frauenheim, T.; Zhang, S.-C. Theoretical prediction of topological insulators in thallium-based III-V-VI_2 ternary chalcogenides. *Euro. Phys. Lett.* **2010**, *90*, 37002.

(12) Lin, H.; Markiewicz, R. S.; Wray, L. A.; Fu, L.; Hasan, M. Z.; Bansil, A. Single-Dirac-Cone Topological Surface States in the $TlBiSe_2$ Class of Topological Semiconductors. *Phys. Rev. Lett.* **2010**, *105*, No. 036404.

(13) Eremeev, S. V.; Koroteev, Yu. M.; Chulkov, E. V. Ternary thallium-based semimetal chalcogenides Tl-V-VI_2 as a new class of three-dimensional topological insulators. *JETP Lett.* **2010**, *91*, 594−598.

(14) Sato, T.; Segawa, K.; Guo, H.; Sugawara, K.; Souma, S.; Takahashi, T.; Ando, Y. Direct Evidence for the Dirac-Cone Topological Surface States in the Ternary Chalcogenide $TlBiSe_2$. *Phys. Rev. Lett.* **2010**, *105*, 136802.

(15) Kuroda, K.; Ye, M.; Kimura, A.; Eremeev, S. V.; Krasovskii, E. E.; Chulkov, E. V.; Ueda, Y.; Miyamoto, K.; Okuda, T.; et al. Experimental Realization of a Three-Dimensional Topological Insulator Phase in Ternary Chalcogenide $TlBiSe_2$. *Phys. Rev. Lett.* **2010**, *105*, 146801.

(16) Chen, Y. L.; Liu, Z. K.; Analytis, J. G.; Chu, J.-H.; Zhang, H. J.; Yan, B. H.; Mo, S.-K.; Moore, R. G.; Lu, D. H.; Fisher, I. R.; et al. Single Dirac cone topological surface state and unusual thermoelectric property of compounds from a new topological insulator family. *Phys. Rev. Lett.* **2010**, *105*, 266401.

(17) Yan, S.; Iaia, D.; Morosan, E.; Fradkin, E.; Abbamonte, P.; Madhavan, V. Influence of Domain Walls in the Incommensurate Charge Density Wave State of Cu Intercalated 1T-$TiSe_2$. *Phys. Rev. Lett.* **2017**, *118*, 106405.

(18) Lian, C.-S.; Si, C.; Wu, J.; Duan, W. First-principles study of Na-intercalated bilayer $NbSe_2$: Suppressed charge-density wave and strain-enhanced superconductivity. *Phys. Rev. B: Condens. Matter Mater. Phys.* **2017**, *96*, 235426.

(19) Teshome, T.; Datta, A. Strain-Induced Topological Insulator in Methyl-Decorated SiGe Films. *J. Phys. Chem. C* **2018**, *122*, 25127−25133.

(20) Teshome, T.; Datta, A. Topological Phase Transition in Sb_2Mg_3 Assisted by Strain. *ACS Omega* **2019**, *4*, 8701−8706.

(21) Teshome, T.; Datta, A. Phase Coexistence and Strain-Induced Topological Insulator in Two-Dimensional BiAs. *J. Phys. Chem. C* **2018**, *122*, 15047−15054.

(22) Hor, Y. S.; Williams, A. J.; Checkelsky, J. G.; Roushan, P.; Seo, J.; Xu, Q.; Zandbergen, H. W.; Yazdani, A.; Ong, N. P.; Cava, R. J. Superconductivity in $Cu_xBi_2Se_3$ and its Implications for Pairing in the Undoped Topological Insulator. *Phys. Rev. Lett.* **2010**, *104*, No. 057001.

(23) Sasaki, S.; Kriener, M.; Segawa, K.; Yada, K.; Tanaka, Y.; Sato, M.; Ando, Y. Topological Superconductivity in $Cu_xBi_2Se_3$. *Phys. Rev. Lett.* **2011**, *107*, 217001.

(24) Kriener, M.; Segawa, K.; Ren, Z.; Sasaki, S.; Ando, Y. Bulk Superconducting Phase with a Full Energy Gap in the Doped Topological Insulator $Cu_xBi_2Se_3$. *Phys. Rev. Lett.* **2011**, *106*, 127004.

(25) Guo, Y.; Zhou, J.; Liu, Y.; Zhou, X.; Yao, F.; Tan, C.; Wu, J.; Lin, L.; Liu, K.; Liu, Z.; et al. Chemical Intercalation of Topological Insulator Grid Nanostructures for High-Performance Transparent Electrodes. *Adv. Mater.* **2017**, *29*, 1703424.

(26) Kitaev, A. Yu Fault-tolerant quantum computation by anyons. *Ann. Phys.* **2003**, *303*, 2−30.

(27) Horcas, I.; Fernández, R.; Gómez-Rodríguez, J. M.; Colchero, J.; Gómez-Herrero, J.; Baro, A. M. WSXM: A software for scanning probe microscopy and a tool for nanotechnology. *Rev. Sci. Instrum.* **2007**, *78*, No. 013705.

(28) Goto, K.; Matsuda, H.; Hashimoto, M.; Nojiri, H.; Sakai, C.; Matsui, F.; Daimon, H.; Toth, L.; Matsushita, T. Development of Display-Type Ellipsoidal Mesh Analyzer. *e-J. Surf. Sci. Nanotechnol.* **2011**, *9*, 311.

(29) Kim, S.; Ye, M.; Kuroda, K.; Yamada, Y.; Krasovskii, E. E.; Chulkov, E. V.; Miyamoto, K.; Nakatake, M.; Okuda, T.; Ueda, Y.; et al. Surface Scattering via Bulk Continuum States in the 3D Topological Insulator Bi_2Se_3. *Phys. Rev. Lett.* **2011**, *10*, No. 056803.

(30) Ye, M.; Eremeev, S. V.; Kuroda, K.; Krasovskii, E. E.; Chulkov, E. V.; Takeda, Y.; Saitoh, Y.; Okamoto, K.; Zhu, S. Y.; Miyamoto, K.; et al. Quasiparticle interference on the surface of Bi_2Se_3 induced by cobalt adatom in the absence of ferromagnetic ordering. *Phys. Rev. B: Condens. Matter Mater. Phys.* **2012**, *85*, 205317.

(31) Tersoff, J.; Hamann, D. R. Theory of the scanning tunneling microscope. *Phys. Rev. B: Condens. Matter Mater. Phys.* **1985**, *31*, 805−813.

(32) Eremeev, S. V.; Vergniory, M. G.; Menshchikova, T. V.; Shaposhnikov, A. A.; Chulkov, E. V. The effect of van der Waal's gap expansions on the surface electronic structure of layered topological insulators. *New J. Phys.* **2012**, *14*, 113030.

(33) Brundle, C. R. The application of electron spectroscopy to surface studies. *J. Vac. Sci. Technol.* **1974**, *11*, 212.

(34) Otrokov, M. M.; Borisova, S. D.; Chis, V.; Vergniory, M. G.; Eremeev, S. V.; Kuznetsov, V. M.; Chulkov, E. V. Efficient step-mediated intercalation of silver atoms deposited on the Bi_2Se_3 surface. *JETP Lett.* **2013**, *96*, 714−718.

(35) Matsui, F.; Matsushita, T.; Kato, Y.; Hashimoto, M.; Inaji, K.; Guo, F.-Z.; Daimon, H. Atomic-layer resolved magnetic and electronic structure analysis of Ni thin film on a Cu(001) surface by diffraction spectroscopy. *Phys. Rev. Lett.* **2008**, *100*, 207201.

(36) Cavallin, A.; Sevriuk, V.; Fischer, K. N.; Manna, S.; Ouazi, S.; Ellguth, M.; Tusche, C.; Meyerheim, H. L.; Sander, D.; Kirschner, J. Preparation and characterization of $Bi_2Se_3(0001)$ and of epitaxial FeSe nanocrystals on $Bi_2Se_3(0001)$. *Surf. Sci.* **2016**, *646*, 72−82.

(37) Otrokov, M. M.; Ernst, A.; Mohseni, K.; Fulara, H.; Roy, S.; Castro, G. R.; Rubio-Zuazo, J.; Ryabishchenkova, A. G.; Kokh, K. A.; Tereshchenko, O. E.; et al. Geometric and electronic structure of the Cs-doped $Bi_2Se_3(0001)$ surface. *Phys. Rev. B: Condens. Matter Mater. Phys.* **2017**, *95*, 205429.

(38) Gosalvez, M. A.; Otrokov, M. M.; Ferrando, N.; Ryabishchenkova, A. G.; Ayuela, A.; Echenique, P. M.; Chulkov, E. V. Low-coverage surface diffusion in complex periodic energy landscapes: Analytical solution for systems with symmetric hops and application to intercalation in topological insulators. *Phys. Rev. B: Condens. Matter Mater. Phys.* **2016**, *93*, No. 075429.

(39) de Jong, N.; Frantzeskakis, E.; Zwartsenberg, B.; Huang, Y. K.; Wu, D.; Hlawenka, P.; Sanchez-Barriga, J.; Varykhalov, A.; van Heumen, E.; Golden, M. S. Angle-resolved and core-level photo-emission study of interfacing the topological insulator $Bi_{1.5}Sb_{0.5}Te_{1.7}Se_{1.3}$ with Ag, Nb, and Fe. *Phys. Rev. B: Condens. Matter Mater. Phys.* **2015**, *92*, No. 075127.

(40) Roy, S.; Polyakov, A.; Mohseni, K.; Meyerheim, H. L. X-Ray Structure Analysis of Ultra - Thin Silver Films on the (0001) Surface

of the Topological Insulator Bi_2Se_3. *Phys. Status Solidi RRL* **2018**, *12*, 1800138.

(41) Blöchl, P. E. Projector augmented-wave method. *Phys. Rev. B: Condens. Matter Mater. Phys.* **1994**, *50*, 17953−17979.

(42) Kresse, G.; Joubert, D. From ultrasoft pseudopotentials to the projector augmented-wave method. *Phys. Rev. B: Condens. Matter Mater. Phys.* **1999**, *59*, 1758−1775.

(43) Kresse, G.; Hafner, J. *Abinitio* molecular dynamics for open-shell transition metals. *Phys. Rev. B: Condens. Matter Mater. Phys.* **1993**, *48*, 13115−13118.

(44) Kresse, G.; Furthmüller, J. Efficiency of ab-initio total energy calculations for metals and semiconductors using a plane-wave basis set. *Comput. Mater. Sci.* **1996**, *6*, 15−50.

(45) Perdew, J. P.; Burke, K.; Ernzerhof, M. Generalized Gradient Approximation Made Simple. *Phys. Rev. Lett.* **1996**, *77*, 3865−3865.

(46) Grimme, S.; Antony, J.; Ehrlich, S.; Krieg, H. A consistent and accurate ab initio parametrization of density functional dispersion correction (DFT-D) for the 94 elements H-Pu. *J. Chem. Phys.* **2010**, *132*, 154104.

(47) Grimme, S.; Ehrlich, S.; Goerigk, L. Effect of the damping function in dispersion corrected density functional theory. *J. Comput. Chem.* **2011**, *32*, 1456−1465.

(48) Teshome, T.; Datta, A. Two-Dimensional Graphene-Gold Interfaces Serve as Robust Templates for Dielectric Capacitors. *ACS Appl. Mater. Interfaces* **2017**, *9*, 34213−34220.

(49) Otrokov, M. M.; Klimovskikh, I. I.; Bentmann, H.; Estyunin, D.; Zeugner, A.; Aliev, Z. S.; Gaβ, S.; Wolter, A. U. B.; Koroleva, A. V.; Shikin, A. M.; et al. Prediction and observation of an antiferromagnetic topological insulator. *Nature* **2019**, *576*, 416−422.

(50) Han, Y.; Tringides, M. C.; Evans, J. W.; Thiel, P. A. Adsorption, intercalation, diffusion, and adhesion of Cu at the $2H$-$MoS_2(0001)$ surface from first-principles calculations. *Phys. Rev. Research* **2020**, *2*, No. 013182.

(51) Roy, S.; Meyerheim, H. L.; Mohseni, K.; Ernst, A.; Otrokov, M. M.; Vergniory, M. G.; Mussler, G.; Kampmeier, J.; Grützmacher, D.; Tusche, C.; et al. Atomic relaxations at the (0001) surface of Bi_2Se_3 single crystals and ultrathin films. *Phys. Rev. B: Condens. Matter Mater. Phys.* **2014**, *90*, 155456.

(52) Jónsson, H.; Mills, G.; Jacobsen, K. W. *Classical and Quantum Dynamics in Condensed Phase Simulations*; Berne, B. J., Ciccotti, G., Coker, D. F., Eds.; World Scientific: Singapore, 1998.

(53) Sheppard, D.; Xiao, P.; Chemelewski, W.; Johnson, D. D.; Henkelman, G. A generalized solid-state nudged elastic band method. *J. Chem. Phys.* **2012**, *136*, No. 074103.